Cell

The Long Noncoding RNA, Jpx, Is a Molecular Switch for X Chromosome Inactivation

Di Tian,[1,2,3] Sha Sun,[1,2] and Jeannie T. Lee[1,2,3,*]
[1]Howard Hughes Medical Institute
[2]Department of Molecular Biology
Massachusetts General Hospital and Department of Genetics, Harvard Medical School, Boston, MA 02115, USA
[3]Department of Pathology, Massachusetts General Hospital, Boston, MA 02114, USA
*Correspondence: lee@molbio.mgh.harvard.edu
DOI 10.1016/j.cell.2010.09.049

SUMMARY

Once protein-coding, the X-inactivation center (*Xic*) is now dominated by large noncoding RNAs (ncRNA). X chromosome inactivation (XCI) equalizes gene expression between mammalian males and females by inactivating one X in female cells. XCI requires Xist, an ncRNA that coats the X and recruits Polycomb proteins. How *Xist* is controlled remains unclear but likely involves negative and positive regulators. For the active X, the antisense Tsix RNA is an established *Xist* repressor. For the inactive X, here, we identify *Xic*-encoded *Jpx* as an *Xist* activator. *Jpx* is developmentally regulated and accumulates during XCI. Deleting *Jpx* blocks XCI and is female lethal. Posttranscriptional Jpx knockdown recapitulates the knockout, and supplying Jpx in *trans* rescues lethality. Thus, *Jpx* is *trans*-acting and functions as ncRNA. Furthermore, *ΔJpx* is rescued by truncating Tsix, indicating an antagonistic relationship between the ncRNAs. We conclude that *Xist* is controlled by two RNA-based switches: Tsix for Xa and Jpx for Xi.

INTRODUCTION

In the mammal, X chromosome inactivation (XCI) achieves dosage balance between the sexes by transcriptionally silencing one X chromosome in the female (Lyon, 1961; Lucchesi et al., 2005; Wutz and Gribnau, 2007; Payer and Lee, 2008; Starmer and Magnuson, 2009). During XCI, ~1000 genes on the X are subject to repression by the X-inactivation center (*Xic*) (Brown et al., 1991). Multiple noncoding genes have been identified within this 100–500 kb domain that, until ~150 million years ago, was dominated by protein-coding genes. The rise of Eutherian mammals and the transition from imprinted to random XCI led to region-wide "pseudogenization" (Duret et al., 2006; Davidow et al., 2007; Hore et al., 2007; Shevchenko et al., 2007). To date, four *Xic*-encoded noncoding genes have been ascribed function in XCI, including *Xist*, *Tsix*, *Xite*, and *RepA* (Brockdorff et al., 1992; Brown et al., 1992; Lee and Lu, 1999; Ogawa and Lee, 2003; Zhao et al., 2008) (Figure 1A). The dominance of ncRNAs brought early suspicion that long transcripts are favored by allelic regulation during XCI and imprinting (for review, see Wan and Bartolomei, 2008; Koerner et al., 2009; Lee, 2009; Mercer et al., 2009). Indeed, the *Xic* region harbors many other ncRNA (Simmler et al., 1996; Chureau et al., 2002), but many have yet to be characterized.

One key player is Xist, a 17 kb ncRNA that initiates XCI as it spreads along the X in *cis* (Brockdorff et al., 1992; Brown et al., 1992; Penny et al., 1996; Marahrens et al., 1997; Wutz et al., 2002) and recruits Polycomb repressive complexes to the X (Plath et al., 2003; Silva et al., 2003; Schoeftner et al., 2006; Zhao et al., 2008). In embryonic stem (ES) cell models that recapitulate XCI during differentiation ex vivo, *Xist* expression is subject to a counting mechanism that ensures repression in XY cells and monoallelic upregulation in XX cells. Prior to differentiation, *Xist* is expressed at a low basal level but is poised for activation in the presence of supernumerary X chromosomes (XX state). In the presence of only one X (XY), *Xist* becomes stably silenced.

It has been proposed that *Xist* is under both positive and negative control (Lee and Lu, 1999; Lee, 2005; Monkhorst et al., 2008). Negative regulation is achieved by the antisense gene, *Tsix*. When *Tsix* is deleted or truncated, the *Xist* allele in *cis* is derepressed (Lee and Lu, 1999; Lee, 2000; Luikenhuis et al., 2001; Sado et al., 2001; Stavropoulos et al., 2001; Morey et al., 2004; Vigneau et al., 2006; Ohhata et al., 2008). *Tsix* represses *Xist* induction by several means, including altering the chromatin state of *Xist* (Navarro et al., 2005; Sado et al., 2005; Sun et al., 2006; Ohhata et al., 2008), deploying Dnmt3a's DNA methyltransferase activity (Sado et al., 2005; Sun et al., 2006), recruiting the RNAi machinery (Ogawa et al., 2008), and interfering with the ability of Xist and RepA RNA to engage Polycomb proteins (Zhao et al., 2008). In turn, *Tsix* is regulated by *Xite*, a proximal noncoding element that interacts with *Tsix*'s promoter (Tsai et al., 2008) and sustains *Tsix* expression on the future Xa (active X) (Ogawa and Lee, 2003).

Significantly, whereas a *Tsix* deletion has major effects on *Xist* in XX cells, it has little consequence in XY cells (Lee and Lu, 1999;

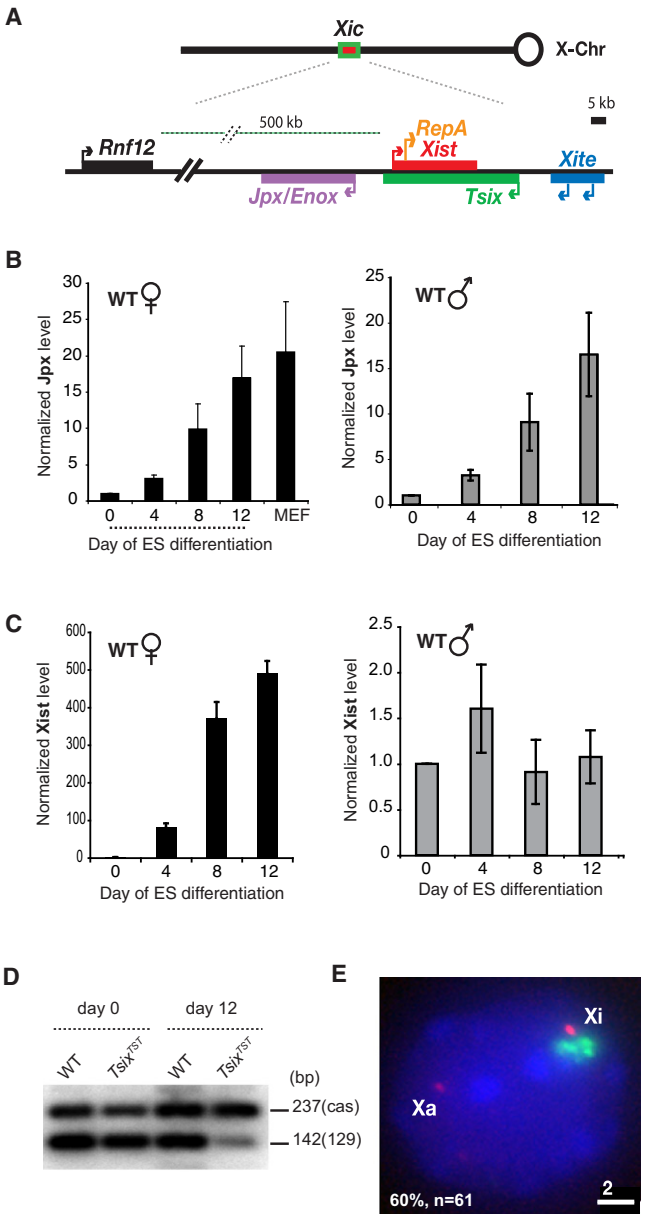

Figure 1. *Jpx* Expression Increases 10- to 20-Fold during ES Cell Differentiation

(A) The *Xic* and its noncoding genes. *Rnf12* is coding and lies 500 kb away.

(B) Time-course analyses of Jpx expression by qRT-PCR in differentiating female and male ES cells. Averages and standard error (SE) from three (female) or four (male) independent differentiation experiments are plotted. Values are normalized to Gapdh RNA and d0 Jpx levels are set to 1.0.

(C) Time-course analyses of *Xist* expression by qRT-PCR in differentiating male and female ES cells. Averages and SE from six (male) and three (female) independent differentiation experiments are plotted. All values are normalized to Gadph RNA and d0 Xist is set to 1.0.

(D) Allele-specific RT-PCR analysis of Jpx in wild-type and $Tsix^{TST}$/+ female ES cells on d0 and d12 of differentiation.

(E) RNA FISH indicates that Jpx escapes inactivation in 60% of d16 female cells. N = 61. Xist clouds are present in 98% of cells. Xist RNA, green. Jpx RNA, red.

Ohhata et al., 2006). This difference led to the idea that *Xist* is not only negatively regulated on Xa but also positively controlled on Xi (inactive X) by factors that activate *Xist* (Lee and Lu, 1999). Positive regulation finds support in that RepA—a short RNA embedded within *Xist*—recruits Polycomb proteins to facilitate *Xist* upregulation (Zhao et al., 2008; Hoki et al., 2009). Activators outside of the *Xist-Tsix-Xite* region must also occur, as an 80 kb transgene carrying only these genes cannot induce XCI (Lee et al., 1999b). Furthermore, female cells carrying a heterozygous deletion of *Xist-Tsix-Xite* still undergo XCI, indicating female cells with only one copy of *Xist*, *Tsix*, and *Xite* still count two X chromosomes (Monkhorst et al., 2008). One such activator has been proposed to be the E3 ubiquitin ligase, Rnf12, whose gene resides ~500 kb away from *Xist* (Jonkers et al., 2009). Overexpression of Rnf12 ectopically induces *Xist* expression in XY cells, but Rnf12 is not required for *Xist* activation in XX cells, as its knockout delays but does not abrogate expression. This implies that essential *Xist* activator(s) must reside elsewhere.

Here, we seek to identify that essential factor. We draw hints from an older study demonstrating that, while transgenes carrying only *Xist-Tsix-Xite* cannot activate *Xist*, inclusion of sequences upstream of *Xist* restores *Xist* upregulation (Lee et al., 1999b). The Eutherian-specific noncoding gene, *Jpx/Enox* (Chureau et al., 2002; Johnston et al., 2002; Chow et al., 2003), lies ~10 kb upstream of *Xist*, is transcribed in the opposite orientation (Figure 1A), but remains largely uncharacterized. *Jpx* lacks open reading frames but is relatively conserved in its 5′ exons. Initial reports indicate that *Jpx* is neither developmentally regulated nor sex specific and is therefore unlikely to regulate XCI (Chureau et al., 2002; Johnston et al., 2002; Chow et al., 2003). Although they imply a pseudogene status, chromosome conformation capture (3C) suggests that *Jpx* resides within *Xist*'s chromatin hub (Tsai et al., 2008). We herein study *Jpx* and uncover a crucial role as ncRNA in the positive arm of *Xist* regulation.

RESULTS

Jpx Escapes XCI and Is Upregulated during ES Cell Differentiation

We first analyzed *Jpx* expression patterns in ES cells, as an *Xist* inducer might be expected to display developmental specificity correlating with the kinetics of XCI. Time-course measurements of Jpx and Xist during ES differentiation into embryoid bodies (EB) showed that Jpx RNA levels increased 10- to 20-fold between d0 and d12 and remained elevated in somatic cells (Figure 1B and data not shown). Upregulation occurred in both XX and XY cells. However, whereas Xist induction paralleled Jpx upregulation in female cells, Xist remained suppressed in male cells (Figure 1C). To determine whether Jpx originated from Xa or Xi, we carried out allele-specific analysis in $Tsix^{TST}$/+ female cells, which are genetically marked by a *Tsix* mutation that invariably inactivates the mutated X of 129 origin (X^{129}) instead of the wild-type *Mus castaneus* X (X^{cas}) (Ogawa et al., 2008). On the basis of a NlaIII polymorphism, RT-PCR demonstrated that both alleles of *Jpx* could be detected from d0 to d12, indicating that *Jpx* escapes XCI (Figure 1D). On d0, there was

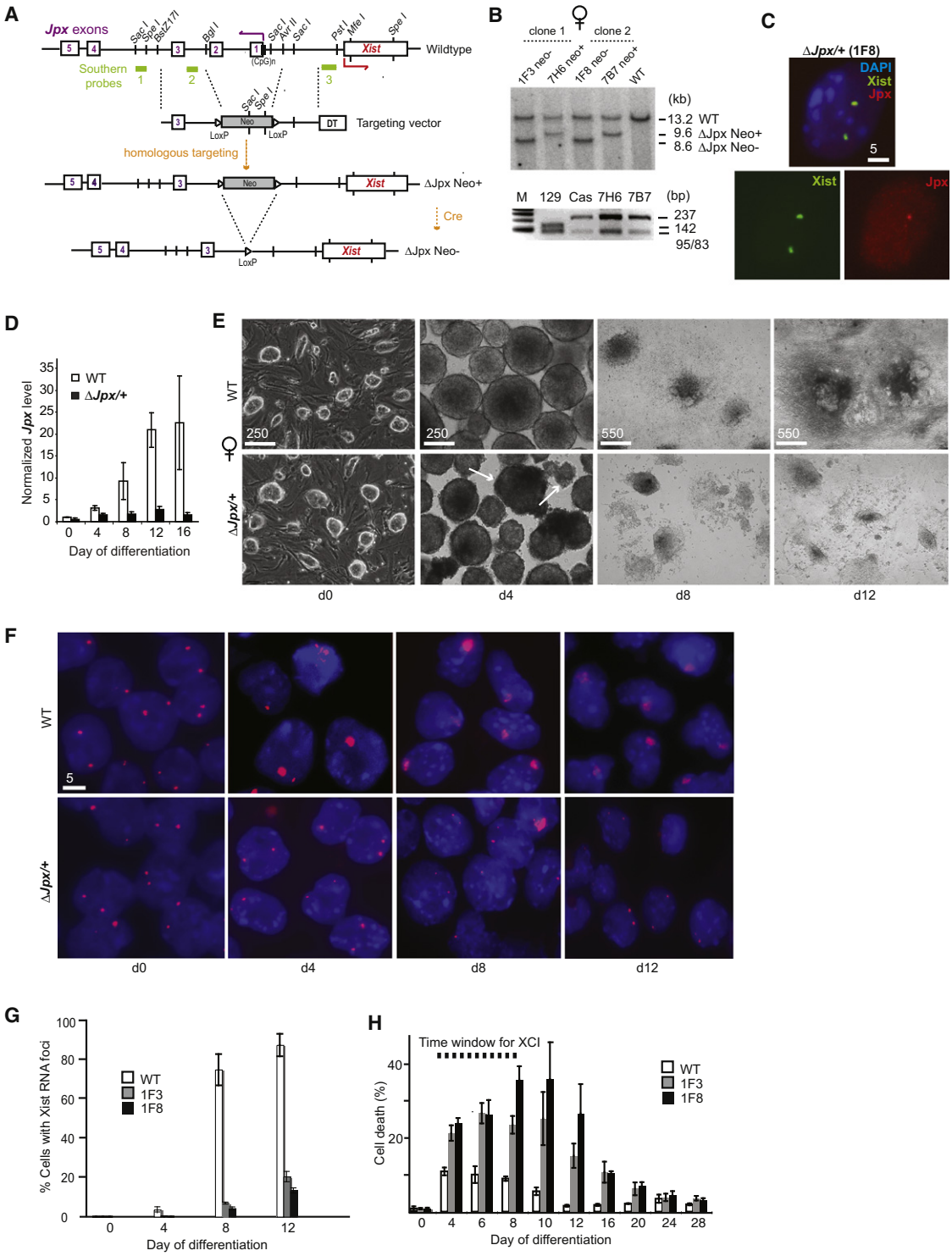

Figure 2. *ΔJpx* Causes Loss of XCI and Massive Cell Death in Female ES Cells

(A) The *Jpx* gene, targeting vector, and products of homologous targeting before and after Cre-mediated excision of the *Neo* positive-selection marker. DT, diphtheria toxin for negative selection. (CpG)n, CpG island. Numbered boxes represent five *Jpx* exons.

(B) Top panel: Southern analysis of SacI-digested genomic DNA from *ΔJpx*/+ and WT female ES cells using probe 1. The Neo- female clones, 1F3 and 1F8, were derived from the Neo+ 6H7 and 7B7 clones, respectively. Bottom panel: Allele-specific PCR analysis showed that the 129 allele was preferentially targeted over the *M. castaneus* (cas) allele. The analysis for Neo+ 6H7 and 7B7 clones are shown. M, 100 bp markers.

(C) DNA FISH of *ΔJpx*/+ female ES cells. *Xist* probe (pSx9), FITC-labeled. The *Jpx* probe (Cy3-labeled, red) is located in the region of deletion.

nearly equal expression from both alleles; between d12 and d16, expression from Xi accounted for 10%–35% of total Jpx.

RNA fluorescence in situ hybridization (FISH) showed that 98% of cells expressed Xist clouds, and Jpx RNA was present on Xi in 60% (Figure 1E, n = 61). In such cells, Jpx RNA was seen on both Xa and Xi. On Xi, Jpx RNA was always adjacent to, not in, the Xist cloud, a juxtaposition characteristic of genes that escape XCI (Clemson et al., 2006; Namekawa et al., 2010). Thus, consistent with previous analysis (Chureau et al., 2002; Johnston et al., 2002; Chow et al., 2003), our results indicate ubiquitous, non-sex-specific Jpx expression. However, our data demonstrate that Jpx upregulation is developmentally regulated to correlate with Xist upregulation, and that *Jpx* significantly escapes XCI.

Deleting *Jpx* Has No Effect on Male Cells but Is Female Lethal

To test *Jpx* function, we knocked out a 5.17 kb region at the 5′ end of *Jpx* that includes its major promoter, CpG island, and first two exons (*ΔJpx*) (Figure 2A and Figure S1A available online). We isolated four independently derived male ES clones and confirmed homologous targeting by Southern analysis using external and internal probes (Figure S1B and data not shown). The *Neo* selectable marker was thereafter removed by Cre-mediated excision. Following DNA FISH to verify the deletion (Figure S1C), we analyzed two independent Neo$^-$ clones for each. Because 1C4 and 1D4 male clones behaved identically, we present data for 1C4 below.

ΔJpx/Y ES cells displayed no obvious phenotype when differentiated into EB to induce XCI. Differentiation in suspension culture from d0 to d4 (day 0 to 4) revealed no morphological anomalies, and adherent outgrowth on gelatin-coated plates after d4 yielded robust growth (Figure S1D). Consistent with this, no elevation of cell death was detected (Figure S1E). RT-PCR analysis showed that *Xist* was appropriately suppressed during differentiation (Figure S1F), RNA FISH confirmed that basal Xist expression became repressed (Figure S1G). Furthermore, the X-linked genes, *Pgk1*, *Mecp2*, and *Hprt*, were all expressed appropriately (Figures S1F and S1G). Strand-specific qRT-PCR showed that Xist and Tsix levels in mutants were not significantly different from those of wild-type cells at any time (Figure S1H). We conclude that deleting *Jpx* has no functional consequence for XY cells.

We also deleted *Jpx* in a hybrid female ES line (16.7) carrying X chromosomes of different strain origin (X^{129}/X^{cas}) (Lee and Lu, 1999). We isolated five independent female clones, verified homologous targeting by Southern analysis using external and internal probes (Figures 2A and 2B and data not shown), and then removed the *Neo* marker by Cre-mediated excision. Allele-specific analysis showed that, in all five cases, X^{129} was targeted (Figure 2B), consistent with the targeting vector's 129 origin. Following DNA FISH to confirm the deletion (Figure 2C), we analyzed two independent Neo$^-$ clones, 1F3 and 1F8. RNA/DNA FISH showed that >95% of mutant cells are XX throughout differentiation. The two female clones behaved similarly.

To quantitate residual Jpx levels in *ΔJpx*/+ cells, we performed qRT-PCR and found less RNA than expected (Figure 2D). On d0, targeting of a single allele resulted in loss of approximately half of Jpx RNA, as expected. However, during differentiation, Jpx levels from the wild-type *castaneus* allele did not increase to the extent anticipated. Between d8 and d16, Jpx was expressed at only 10%–20% of wild-type levels (50% expected). This disparity could not be explained by strain-specific differences, as allele-specific analysis of wild-type cells demonstrated similar allelic levels between d0 and d12 (Figure 1D). Deleting one *Jpx* allele therefore resulted in effects on the homologous allele, suggesting an expression feedback loop. Thus, a heterozygous deletion severely compromises overall *Jpx* expression and approximates a homozygous deletion.

To investigate effects on XCI, we differentiated ES cells into EB to induce XCI. Although *ΔJpx*/+ and wild-type cells were indistinguishable on d0, differentiation uncovered profound effects. Wild-type EB typically showed smooth and radiant borders between d2 and d4 when grown in suspension, but mutant EB exhibited necrotic centers, irregular edges, and disaggregation (Figure 2E, arrows). The difference became more obvious during the adherent phase (post-d4). Whereas wild-type EB adhered to plates and displayed exuberant cellular outgrowth, mutant EB attached poorly and showed scant outgrowth. The difference was not due to *Jpx* effects on cell differentiation per se, as immunostaining of stem cell markers showed that mutant EB appropriately downregulated Oct4 and Nanog upon differentiation (Figure S2). Thus, whereas *ΔJpx* had little effect in males, deleting one *Jpx* allele in females caused severe abnormalities during differentiation.

The female-specific nature suggested a link to XCI, a process tightly coupled to cell differentiation (Monk and Harper, 1979; Navarro et al., 2008; Donohoe et al., 2009). To test this possibility, we performed a time-course analysis of Xist expression by RNA FISH (Figures 2F and 2G). In wild-type cells, XCI was largely established by d8–d12, with 75.0% ± 4.8% (mean ± SE) of female cells displaying large Xist clusters by d8 and 89.1% ± 3.4% by d12. However, in *ΔJpx*/+ cells, *Xist* upregulation was severely compromised, with only 6.35% ± 1.77% displaying Xist foci on d8 and no major increase on d12. Strand-specific RNA FISH confirmed that large RNA clouds

(D) Time-course analyses of Jpx expression by qRT-PCR in differentiating WT and *ΔJpx*/+ female ES cells. Averages and standard errors (SE) from three independent differentiation experiments are plotted, with values normalized first to Gapdh and then d0 WT *Jpx* levels are set to 1.0.

(E) Brightfield photographs of WT and *ΔJpx*/+ female ES cells from d0 to d12 of differentiation. Arrows point to disintegrating, necrotic EBs present in mutant cultures.

(F) RNA FISH to examine the time course of Xist upregulation. Xist probe, Cy3-labeled pSx9.

(G) Plotted time course of Xist upregulation in WT and two *ΔJpx*/+ mutants, 1F3 and 1F8. Averages ± SE from three independent differentiation experiments are shown. Sample sizes (n): d0, 595–621; d4, 922–1163; d8, 3013–4370; d12, 3272–4794.

(H) Massive cell death in mutant female cells. The trypan blue staining results of three independent differentiation experiments were averaged and plotted with SE d0, n = 150–800 cells for d0; d4, n = 200–500 cells; all other time points, n = 500–2000 cells.

See also Figures S1– S3.

during differentiation were of Xist origin and residual pinpoint signals were of Tsix (Figure S3). The Xist deficiency mirrored poor EB growth and massive cell death over the same time course (Figures 2E and 2G). The disparity was greatest between d4 and d12, when mutant cell death approached ten times that of wild-type cells (Figure 2H). Between d4 and d12, at least 85% of mutant cells were lost. Because dead cells detached from culture, the actual percentage of Xist$^+$ cells was probably even lower (< < 6%) than measurable by collecting attached cells for RNA FISH.

Our data argue that *Jpx* is an activator of *Xist*. *ΔJpx* differs from *ΔRnf12*, which merely delays *Xist* induction by two days and does not prevent XCI (Jonkers et al., 2009). We believe that *ΔJpx* blocks XCI rather than delays it, because Xist clouds were rare up to d16. Whereas *ΔRnf12*/+ cells are fully capable of expressing Xist, *ΔJpx*/+ cells have severely compromised Xist expression at all time points. Moreover, whereas *ΔRnf12*/+ cells are viable, *ΔJpx*/+ cells undergo massive cell death during differentiation. Therefore, *Jpx* serves an essential function and precludes Xist induction when deficient.

Jpx Acts in *trans*

Interestingly, *ΔJpx*'s influence on *Xist* was not restricted in *cis* to X^{129} but also blocked *Xist* upregulation on X^{cas}, implying that, unlike other *Xic*-encoded factors, *Jpx* may be *trans*-acting. If so, expressing *Jpx* from an autosomal transgene might rescue *ΔJpx*/+ cells. To test this, we introduced a 90 kb BAC carrying full-length *Jpx* (and no other intact gene) (Figure 3A) into *ΔJpx*/+ cells (1F8) and characterized two independent clones, *Jpx*+/−;TgB2 and *Jpx*+/−;TgB3. Both clones carried autosomal insertions, and qPCR using primer pairs at different transgene positions indicated that each clone carried one to two copies of the full-length transgene (Figure 3B and data not shown). In both clones, Jpx levels were restored between d0 and d12 (Figure 3C).

Significantly, both clones behaved differently from *ΔJpx*/+ cells and were more similar to wild-type cells. Whereas *ΔJpx*/+ cells differentiated poorly and displayed elevated cell death, *Jpx*+/−;TgB2 and *Jpx*+/−;TgB3 cells differentiated well and were fully viable (Figures 3D and 3E). Moreover, *Xist* expression was fully restored in *Jpx*+/−;TgB2 and *Jpx*+/−;TgB3 cells, both in steady-state levels and in the number of cells with Xist clouds (Figures 3F–3H). We conclude that an autosomal *Jpx* transgene rescues the X-linked *Jpx* deletion and that *Jpx* must therefore be able to act in *trans*.

Jpx Acts as a Long ncRNA

In principle, *Jpx* could function as a positive regulator in several ways. *Jpx* could operate as enhancer, given 3C analysis showing interaction between *Jpx* and *Xist* within a defined chromatin hub (Tsai et al., 2008). However, a luciferase reporter assay in stably transfected female ES cells uncovered no obvious enhancer within the deleted *Jpx* region (Figure S4). In this assay, *Jpx* not only failed to enhance luciferase expression but actually depressed it in some cases. A relative increase in expression occurred between d0 and d2, but activation never exceeded that of the *Xist*-only construct. While we cannot exclude an enhancer, enhancer function would be difficult to reconcile with *Jpx*'s *trans* effects.

Jpx's *trans*-acting property might be better explained by a diffusible ncRNA. To distinguish RNA-based mechanisms from those of DNA, chromatin, and/or transcriptional activity, we used shRNA to deplete Jpx RNA after it is transcribed and to knock down both *Jpx* alleles. We generated clones of wild-type female ES cells carrying one of three Jpx-specific shRNAs directed against nonpolymorphic regions of exon 1 (Figure 4A: shRNA-A, -B, -C) and analyzed two to three independent clones with good knockdown efficiency for each (e.g., shRNA-A1, -A2, -A3). Controls carrying scrambled shRNA (Scr) were generated and analyzed in parallel. Using qRT-PCR with primer pairs positioned in exon 1, we observed 70%–90% depletion of Jpx RNA (Figure 4B). Allele-specific RT-PCR showed that 129 and *castaneus* alleles were symmetrically targeted (Figure 4C). Because all clones behaved similarly, results are shown for representative clones.

Phenotype analysis indicated that all knockdown clones recapitulated *ΔJpx*. Knockdown clones grew indistinguishably from wild-type on d0 and only lost viability upon differentiation (Figures 4D and 4E). Between d0 and d4, EB formed by shRNA clones were inferior in size and quality to those of wild-type and Scr control (Figure 4E). Between d4 and d12, knockdown EB showed poor outgrowth and underwent massive cell death at magnitudes comparable to those for *ΔJpx*/+ cells (Figures 4D and 4E). Xist RNA FISH indicated a deficiency of Xist$^+$ cells in differentiating knockdown clones (Figures 4F and 4G). Similarly, qRT-PCR demonstrated significantly lower Xist levels when Jpx RNA was knocked down by *Jpx*-specific shRNAs (Figure 4H). These data showed that targeting both Jpx alleles for posttranscriptional RNA degradation recapitulates the heterozygous deletion.

In *ΔJpx*/+ cells, only 10%–20% of Jpx RNA remained, though the *castaneus* allele was not deleted. To determine the consequences of further Jpx deletion, we introduced shRNA-C into the heterozygous cells (1F8) and depleted Jpx RNA by another ~50% (Figure 4I). Further depletion did not worsen the already severe phenotype, as Xist upregulation remained similarly compromised and EB viability remained poor (Figure 4I), possibly because Jpx was already largely abrogated. Thus, posttranscriptional depletion of Jpx RNA achieves the equivalent of the *Jpx*−/−state (~10% residual RNA) and argues that *Jpx* acts as a long ncRNA.

Jpx Has a Mild *cis* Preference

While *ΔJpx* eliminated almost all female cells during differentiation, a very small subset persisted past d20 and continued to proliferate, indicating that rare cells might bypass *ΔJpx.* To investigate the XCI status of surviving cells, we expanded survivors to d28, performed Xist RNA FISH, and found that Xist induction occurred in almost all survivors (Figure 5A). To ask which of two *Xist* alleles was upregulated, we performed allele-specific RNA-DNA FISH and observed that *Xist* was induced monoallelically from X^{129} or X^{cas} (Figure 5B; RNA/DNA FISH showed that >95% of mutant cells are XX; only XX cells were counted). However, X^{cas} was favored by a ratio of 65:35 in d28 survivors (Figure 5C), indicating that *ΔJpx* is a disadvantage for the *Xist* allele linked to it. Allele-specific RT-PCR of Xist, Pgk1, Mecp2, and Hprt ratios confirmed these findings (Figure 5D).

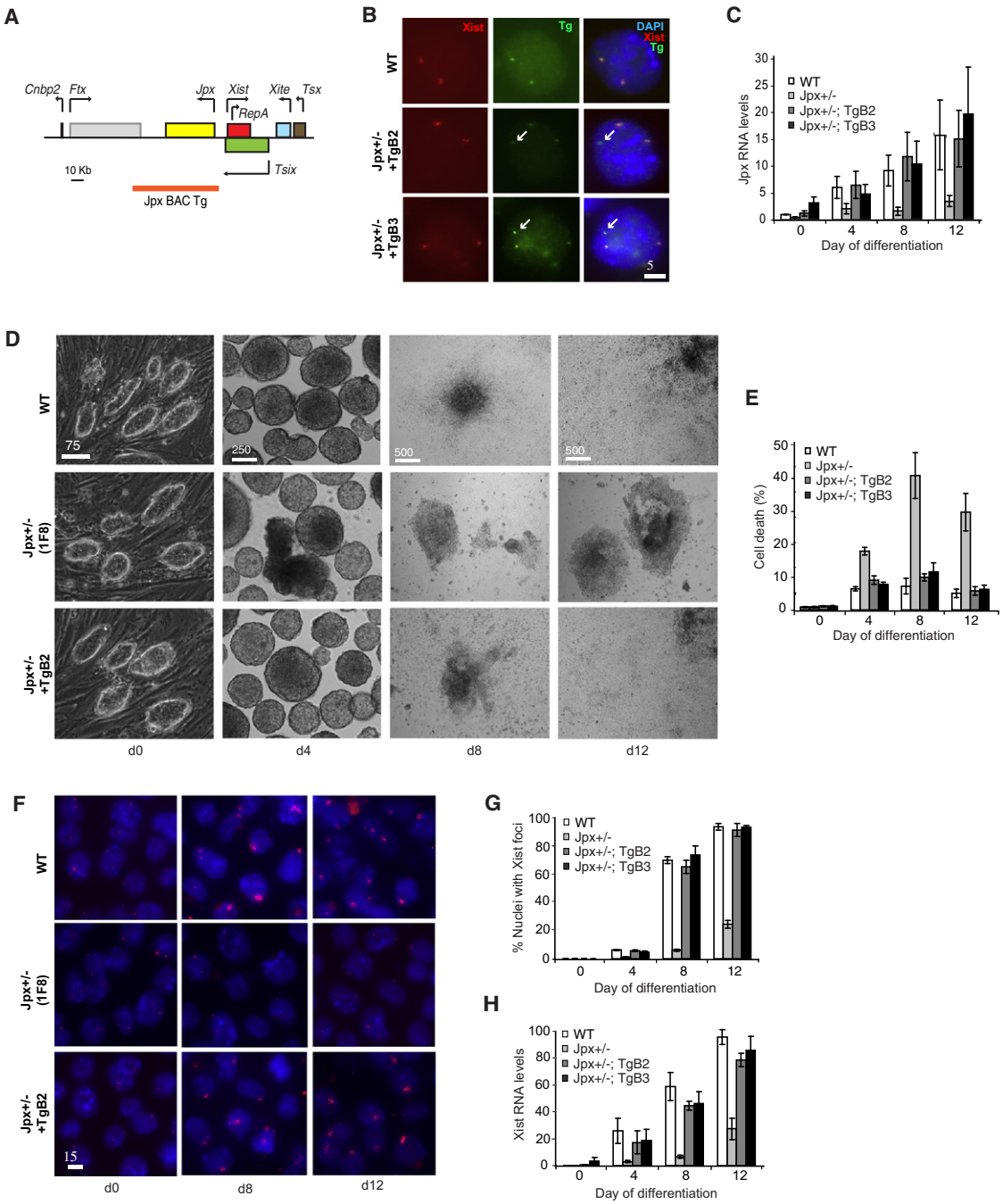

Figure 3. Transgenic *Jpx* Rescues *ΔJpx* in *trans*

(A) Map of the Xic and 90 kb *Jpx* transgene.

(B) Multiprobe DNA FISH to localize *Xist* (pSx9, red) and *Jpx* (BAC, green) in two independent transgenic clones, TgB2 and TgB3. Arrows, *Jpx* transgene.

(C) Time-course analyses of Jpx expression by qRT-PCR in differentiating cells of indicated genotype. Averages ± SE from three independent differentiation experiments are plotted. Values are normalized to Gapdh RNA and WT d0 Jpx level is set to 1.0.

(D) Brightfield photographs of WT and transgenic EB from d0 to d12.

(E) Cell death analysis of WT, knockout, and transgenic EB, performed as above.

(F) RNA FISH to examine the time course of Xist upregulation. Xist probe, Cy3-labeled pSx9.

(G) Quantitation of WT, knockout, and transgenic EB with Xist RNA foci (RNA FISH) from d0 to d12.

(H) qRT-PCR of steady-state Xist levels in WT, knockout, and transgenic EB from d0 to d12.

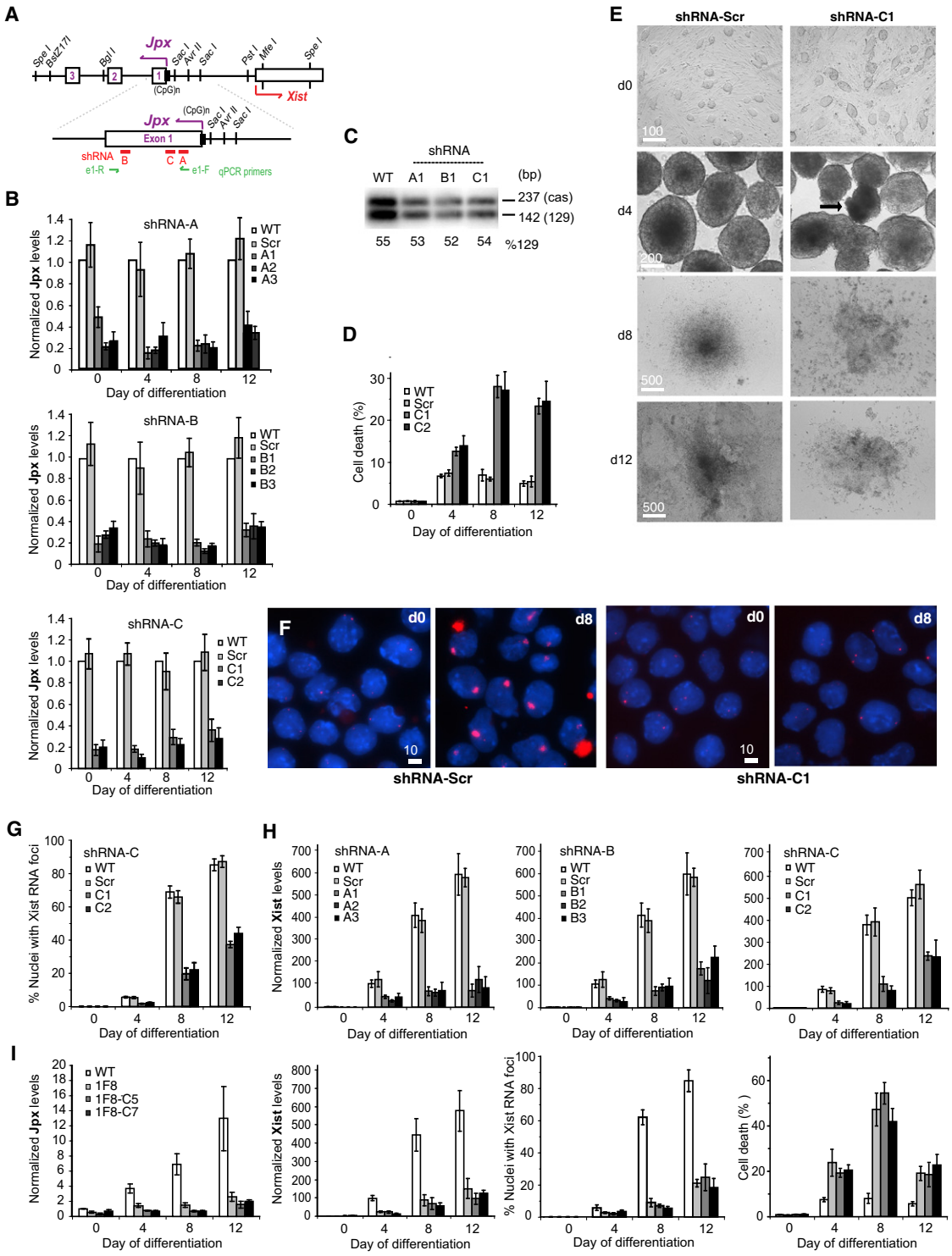

Figure 4. *Jpx* Functions as a Long ncRNA

(A) A map of the 5′ end of *Jpx* showing its exons (purple), shRNA locations, and qPCR primer positions.

(B) Significant knockdown of Jpx RNA in two to three independent clones for each *Jpx*-specific shRNA, but not in the scrambled shRNA clone (Scr). Jpx RNA levels are normalized to WT levels for each day of differentiation. A1–A3 are clones for shRNA-A; B1–B3 for shRNA-B; and C1, C2 for shRNA-C.

(C) Residual Jpx RNA was extracted from d8 shRNA clones, A1, B1, and C1, and subjected to allele-specific RT-PCR (NIa-III polymorphism). The gel was blotted and hybridized to an end-labeled oligo. Allelic fractionation shows similar ratios of 129:*castaneus* bands in WT and knockdown clones, suggesting that the

RNA FISH also demonstrated that Xist upregulation led to silencing of genes in *cis* (Figure 5E), demonstrating that *Jpx* does not affect gene silencing per se. The observed allelic biases were the opposite of wild-type, which ordinarily favors inactivating X^{129} due to the strain-specific *Xce* modifier (Cattanach and Isaacson, 1967). Thus, although *trans*-acting, *Jpx* has a measurable *cis* preference that is uncovered only in rare female survivors (Figure 5F).

Antagonism between *Tsix* and *Jpx* in the Control of *Xist*

Several models for *Xist* regulation postulate a balancing act between positive and negative factors (Lee and Lu, 1999; Lee, 2005; Monkhorst et al., 2008; Navarro et al., 2008; Donohoe et al., 2009; Starmer and Magnuson, 2009; Ahn and Lee, 2010). *Xite* and *Tsix* clearly reside in the repressive regulatory arm (Lee and Lu, 1999; Sado et al., 2001; Ogawa and Lee, 2003). *ΔJpx*'s phenotype suggests that *Jpx* may reside in a parallel, opposing arm. To test the idea of *Jpx* and *Tsix* antagonism, we targeted the $Tsix^{TST}$ mutation (Ogawa et al., 2008) into *ΔJpx*/+ cells to truncate Tsix RNA on the chromosome bearing *ΔJpx* (Figure 6A). Targeting was confirmed by Southern blot analysis and allele-specific genotyping (Figure 6B and data not shown). Intriguingly, truncating Tsix almost completely restored viability and differentiation of *ΔJpx*/+ cells. Cell death analysis showed that two independently derived double mutants, 1F8-S1 and 1F8-S2, have reduced cell death between d6 and d12 when compared to the single mutant (Figure 6C). Cell death was comparable to that of wild-type EB, though significantly higher between d4 and d6. Furthermore, unlike single mutants, double mutants exhibited normal EB morphology and outgrowth (Figure 6D) and RNA FISH showed restoration of *Xist* upregulation and kinetics (Figures 6E and 6F). These results demonstrate that $Tsix^{TST}$ suppresses *ΔJpx*.

We next asked how allelic choice was further affected in *Jpx-Tsix* double mutants. Single mutations both skew XCI ratios, but the polarity is opposite: $Tsix^{TST}$/+ cells exclusively inactivate X^{129} (Ogawa et al., 2008), whereas *ΔJpx*/+ survivors preferentially inactivate X^{cas} (Figure 5). In the double mutant, allele-specific RT-PCR for *Xist*, *Pgk1*, and *Mecp2* expression revealed *Tsix*'s dominance over *Jpx* (Figure 6G). Abrogating Tsix RNA not only overcame the block to transactivate *Xist*, but also skewed choice to favor X^{129}. Therefore, when Tsix RNA is eliminated, the linked *Xist* allele is induced despite a Jpx deficiency. To determine whether further reduction of Jpx by shRNA knockdown affected the rescue, we introduced shRNA-C into the double mutant but did not observe additional effects on Xist expression or cell viability (Figures 6H and 6I).

In principle, the rescue of *ΔJpx* by $Tsix^{TST}$ could be interpreted in two ways. One idea is that *Tsix* and *Jpx* reside a single genetic pathway in which *Jpx* occurs upstream of *Tsix* and controls *Xist* expression by suppressing *Tsix*'s repressive effect on *Xist*. We do not favor this idea, given that deleting *Jpx* did not affect Tsix levels in male cells (Figure S1H). Moreover, the *Tsix-Jpx* double mutant was not identical in phenotype to $Tsix^{TST}$, as the double mutant still demonstrated elevated cell death at early time points in spite of rescuing *Xist* expression (Figure 6C). Thus, we believe that the data collectively argue for parallel pathways in which *Tsix* and *Jpx* independently control *Xist* transcription. In this scenario, how can Xist be induced in double mutants? One possibility is that residual Jpx levels from X^{cas} were sufficient to activate Xist in *trans*. This alone cannot explain the rescue, however, as residual Jpx from X^{cas} could not upregulate *Xist* at all in *ΔJpx*/+ cells (Figures 2D, 2F, and 2G). We propose that eliminating the negative arm of regulation (via $Tsix^{TST}$) created a hyper-permissive state for Xist upregulation in which even very low Jpx expression might be sufficient to induce Xist expression.

DISCUSSION

Our work demonstrates that *Xist* is controlled by two parallel RNA switches—Tsix for Xa and Jpx for Xi. Whereas Tsix represses *Xist* on Xa, Jpx activates *Xist* on Xi. How Jpx RNA transactivates *Xist* is yet to be determined, but it is intriguing that expression of one long ncRNA would be controlled by another. Recapitulation of the knockout by posttranscriptional knockdown of Jpx implies that the activator acts as an RNA. Unlike other ncRNAs of the *Xic*, Jpx is *trans*-acting and diffusible. Indeed, autosomally expressed Jpx RNA can rescue the X-linked *ΔJpx* defect. We cannot exclude the possibility that *Jpx* also acts as an enhancer, though our reporter assay did not uncover such a property (Figure S4). Interestingly, 3C analysis previously revealed close chromatin contact between the 5′ ends of *Jpx* and *Xist* in *cis* (Tsai et al., 2008). Their physical proximity may underlie *Jpx*'s preference for the linked *Xist* allele (Figure 5), as a diffusion-limited Jpx RNA would be expected to preferentially bind the *Xist* allele closer to it.

Our findings place *Jpx*'s function in an epistatic context (Figure 7A). Prior work has proposed that *Xite* and *Tsix* reside at the top of the repressive pathway, controlling XCI counting

shRNAs affected both Jpx alleles. Only 10%–30% of Jpx RNA was left in the knockdowns and therefore the PCR was overcycled to visualize the low residual levels of Jpx in the knockdown cells.

(D) Cell death assay shows that loss of Jpx RNA reduces cell viability during differentiation. Clones shRNA-C1 and -C2 are shown, but shRNA-A and -B clones also show increased cell death.

(E) Brightfield images show poor EB formation and outgrowth in knockdowns but not Scr control.

(F) Xist RNA FISH shows loss of Xist upregulation when Jpx is knocked down using shRNA-C.

(G) Quantitation of the number of cells with Xist RNA clusters from three independent differentiation experiments of control and knockdown clones. Average ± SE shown.

(H) Quantitation of Xist RNA levels in control and knockdown clones from three independent differentiation experiments. RNA levels are normalized to d0 WT values. Average ± SE shown. Differentiation of shRNA-A and -B knockdown clones were performed at the same time; therefore, WT and Scr values for shRNA-A and shRNA-B are the same.

(I) Jpx knockdown in *ΔJpx*/+ cells (1F8) using shRNA-C. Independent clones, C5 and C7, behaved similarly to each other and also to their parent, 1F8, in all assays shown. Average ± SE shown. All values are normalized to d0 WT.

See also Figure S4.

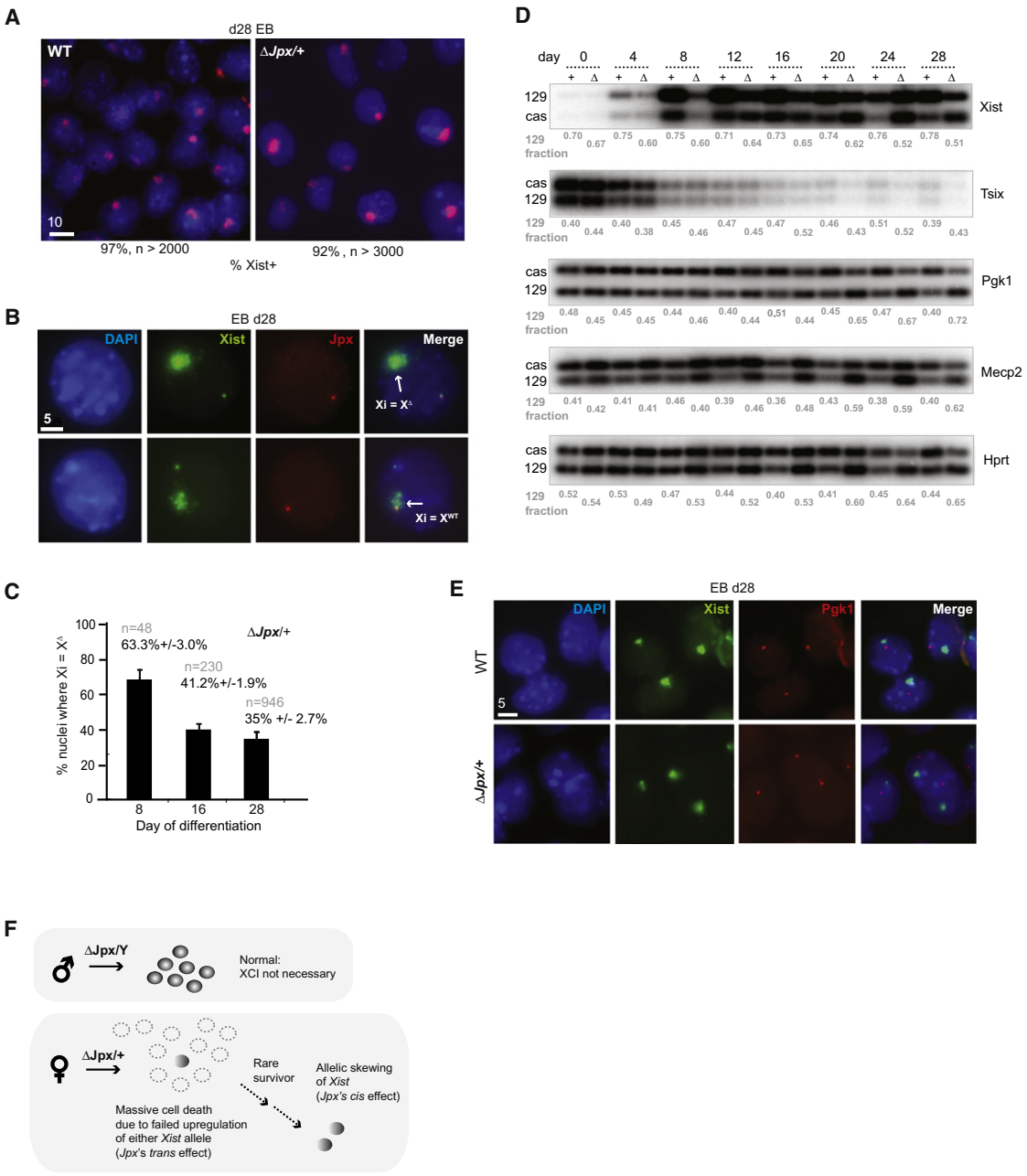

Figure 5. *Jpx*'s Mild *cis* Preference Revealed in *ΔJpx*/+ Survivors

(A) Xist RNA FISH on d28 EB. Xist probe, Cy3-labeled pSx9. WT, 97% Xist$^+$ cells (n > 2000). *ΔJpx*/+, 92% Xist$^+$ cells (n > 3000).

(B) Allele-specific RNA/DNA FISH determines which X is Xi. FITC-labeled pSx9 probe detects Xist RNA and the *Xist* locus from both Xs, whereas the Cy3-labeled *Jpx* probe detects only the wild-type X (the probe resides in the deleted region).

(C) Percentage of 1F8 mutant female cells where Xi = X$^{\Delta}$ (i.e., X^{129}). Averages ±SE from three independent differentiation experiments.

(D) Allele-specific RT-PCR of indicated transcripts from d0 to d28. The percentage of transcripts from the 129 allele (%129) is determined by phosphorimaging. +, WT. Δ, 1F8 mutant. Values for lanes that are not visible are obtained after a longer exposure.

(E) Two-color RNA FISH for Xist and Pgk1 transcripts in d28 cells.

(F) Summary of *ΔJpx* effects on male and female ES cells.

and choice by inducing homologous chromosome pairing through Oct4 (Bacher et al., 2006; Xu et al., 2006; Donohoe et al., 2009). X-X pairing would play an essential role in breaking epigenetic symmetry by shifting the binding of *Tsix*- and *Xite*-associated transcription factors from both X's to the future Xa (Xu et al., 2006; Nicodemi and Prisco, 2007; Donohoe et al., 2009; Lee, 2009). Retained transcription factors would then sustain *Xite* and *Tsix* expression and block *Xist* activation on

Xa (Stavropoulos et al., 2001; Ogawa and Lee, 2003), in part by interfering with the action of RepA RNA and Polycomb proteins (Sun et al., 2006; Zhao et al., 2008).

Work from the current study supports the existence of a parallel, but activating pathway for establishment of Xi. *Jpx* resides in this pathway (Figure 7A). The RNA is upregulated 10- to 20-fold during ES differentiation and leads to monoallelic *Xist* induction in female cells. The collective evidence suggests that Jpx and RepA RNA collaborate to transcriptionally activate *Xist*. In this model, loss of *Tsix* expression on the future Xi would enable the RepA-Polycomb complex to load onto the *Xist* chromatin and trimethylate H3-K27 on the *Xist* promoter (Zhao et al., 2008), creating a permissive state in which Jpx RNA could transactivate *Xist*.

In male cells, Jpx upregulation does not result in *Xist* induction on the single X—similar to the Xa of female cells. As would be the case for the female Xa, persistence of Tsix in male cells overrides Jpx by recruiting silencers to the *Xist* promoter (Navarro et al., 2005; Sado et al., 2005; Sun et al., 2006). In the context of Tsix regulation, DNA methylation and RNAi have been invoked in *Xist* silencing (Norris et al., 1994; Ariel et al., 1995; Zuccotti and Monk, 1995; Sado et al., 2005; Sun et al., 2006; Ogawa et al., 2008). By this model, female cells deficient for Jpx would be unaffected on d0 because *Jpx* is normally not induced until cell differentiation and the onset of XCI. Once induced, Jpx RNA remains at high levels in somatic cells (Figure 1), implying that continued presence of the activator may be necessary for lifelong *Xist* expression in the female. *Jpx* may also play other roles during development, given that the *Tsix-Jpx* double mutant rescues *Xist* expression but does not fully rescue cell death (Figure 6).

In conclusion, our study identifies *Jpx* as an RNA-based activator of *Xist* and supports a dynamic balance of activators and repressors for XCI control. The fate of *Xist* appears to be determined by a series of *Xic*-encoded RNA switches, reinforcing the idea that long ncRNAs may be ideally suited to epigenetic regulation involving allelic and locus-specific control (Lee, 2009). Future work will help elucidate why the *Xic*, once protein-coding, was replaced in recent evolutionary history by noncoding genes.

EXPERIMENTAL PROCEDURES

Construction of *ΔJpx* Cell Lines

Male (J1) and female (16.7) ES cell lines, culture condition, and cell differentiation protocols have been described (Lee and Lu, 1999). To generated *ΔJpx*, a 5′ homology arm (6.5 kb BstZ17I-BglI of *Jpx*) was cloned into the NotI site of vector, PgkNeo2LoxDTA. To the resulting vector was cloned the 3′ arm (6.19 kb AvrII-PstI fragment) into the NheI-SalI site, yielding a 5.17 kb deletion. The targeting construct was linearized with XhoI and electroporated. For screening, ~2000 male and ~2500 female G418-resistant clones were picked, and 4 male and 5 female independent knockout clones were analyzed. To excise the *Neo* selection marker, a Cre plasmid (pMC-CreN) was introduced and G418-sensitive colonies identified. Homologous targeting was confirmed by genomic Southern blots using 5′ and 3′ external probes, as well as internal probes to rule out ectopic integrations. The templates for 5′ and 3′ external probes were PCR products generated using primers: GAGCTCTGAGACA CAGCGCAA and GCCAAAGGGGTTGTCATCTATG for the 5′ probe (nt 84779–85380 of GenBank sequence AJ421479); and GCCCAGGAACTGA GTTTTAGCACA and TGCTTATGGACGATCAAAGTGCC for the 3′ probe (nt 104761–105450 of AJ421479). To determine which allele was targeted in females, we carried out allele-specific PCR analysis based on a NlaIII polymorphic site at nt 95,738 (GenBank sequence AJ421479) within *Jpx* (CATG for the 129; CAAG for *castaneus*). Genomic DNA was amplified by primer pairs, JpxUp (cggcgtccacatgtatacgtcc) and JpxLo (taggaatgagcctccccagcct) (Chureau et al., 2002), to generate a 329 bp product (nt 95598–95926 of GenBank AJ421479), which was then digested with NlaIII to yield 142, 95, 83, and 9 bp fragments for 129 and 237, 83, and 9 bp fragments for *castaneus*. All female clones showed targeting of the 129 allele.

Generation of Transgenic *Jpx* Cell Lines

A 90 kb BAC transgene containing full-length *Jpx* (and no other known transcribed sequences) and a *Neo* resistance marker was made by ET-cloning (Yang and Seed, 2003) from BAC clone 399K20 (Invitrogen). Ten million 1F8 cells (*ΔJpx*/+) were electroporated with 20 μg linearized BAC DNA and cultured under G418 selection (250 μg/ml). Two G418-resistant clones (TgB2 and TgB3) were picked on d8 and expanded for analysis.

Generation of *Tsix^{TST} ΔJpx/ ++* ES Cells

The *Tsix^{TST}* truncation vector has been described (Ogawa et al., 2008). The *ΔJpx*/+ female line, 1F8, was electroporated with the *Tsix^{TST}* vector, 96 clones were picked after puromycin selection, and targeting into X^{129} was determined by Southern blot analysis and allele-specific PCR, as described (Ogawa et al., 2008). Two independent clones, 1F8-S1 and 1F8-S2, were analyzed in parallel.

Generation of Jpx Knockdown Clones

To generate three shRNA knockdown plasmids, three nonpolymorphic sequences from *Jpx* exon 1 were inserted into the EcoRI and *NheI* site of pLKO1 (Addgene): shRNA-A, 5′-CCGGcaccaggcttctgtaacttatCTCGAGataa gttacagaagcctggtgTTTTTG-3′; shRNA-B, 5′-CCGGtagaggatgacttaataagga CTCGAGtccttattaagtcatcctctaTTTTTG-3′; and shRNA-C: 5′-CCGGGGCGT CCACATGTATACGTCCCTCGAGGGACGTATACATGTCGACGCCTTTTTG-3′. 16.7 cells were electroporated with either Jpx-specific or a scrambled (Scr) shRNA vector and selected with puromycin for stable integration. Multiple independent clones were picked (24 for shRNA-A, 24 for shRNA-B, and 48 for shRNA-C) and tested for Jpx knockdown efficiency by qRT-PCR (see Quantitative RT-PCR). We analyzed two to three independent clones for each.

RNA and DNA FISH

FISH protocols and probes (*Xist*, *Pgk1*) have been described (Lee and Lu, 1999; Stavropoulos et al., 2001). The *Jpx* probe is a 3.7 kb fragment (nt 93362–97039 of GenBank AJ421479) within the deleted region that was cloned into pCR-Blunt II-Topo vector (Invitrogen) for Nick translation. For two-color strand-specific RNA FISH, an FITC-labeled Xist riboprobe cocktail was generated by in vitro transcription (MAXIscript kit, Ambion) to detect the Xist strand, and Tsix was detected by Cy3-labeled pCC3, a 5′ Tsix probe that does not overlap *Xist* (Lee et al., 1999a; Ogawa and Lee, 2003).

Quantitative RT-PCR

Real-time PCR for Xist, Tsix, and Jpx was performed under the following conditions: 95°C 3 min; 95°C 10 s, 60°C 20 s, 72°C 20 s, for a total of 40 cycles, and 72°C 5 min. Melting curves for primer pairs were determined by increasing temperatures from 60°C to 95°C at 0.5°C interval for 5 s. Primers for Xist qRT-PCR were NS66 and NS33, and for Tsix NS18 and NS19 (Stavropoulos et al., 2001). Primers for Jpx were *e1*-F, GCACCACCAGGCTTCTGTAAC, and *e1*-R, GGGCATGTTCATTAATTGGCCAG.

Allele-Specific RT-PCR

Allele-specific RT-PCR was performed as described (Stavropoulos et al., 2001; Ogawa and Lee, 2003). Total RNA was extracted by Trizol (Invitrogen) and DNA was removed with DNase I treatment (Ambion). Reverse transcription was then performed with SuperScript III First Strand Synthesis System (Invitrogen). Allele-specific primers were: NS66 and NS33 for *Xist* (Stavropoulos et al., 2001), NS18 and NS19 for *Tsix* (Stavropoulos et al., 2001), NS43 and NS44 for *Mecp2* (Ogawa and Lee, 2003), KH106 and KH107 for *Pgk1* (Huynh and Lee, 2003), and NS41 and NS70 for *Hprt* (Stavropoulos et al., 2001). Southern blot was carried out using nested primers as probes as referenced above: XSP1 for *Xist*, NS19 for *Tsix*, NS65 for *Mecp2*, KH106 for *Pgk1*, and NS59 for *Hprt*. For Jpx allele-specific RT-PCR, Jpx cDNA was amplified with JpxLow

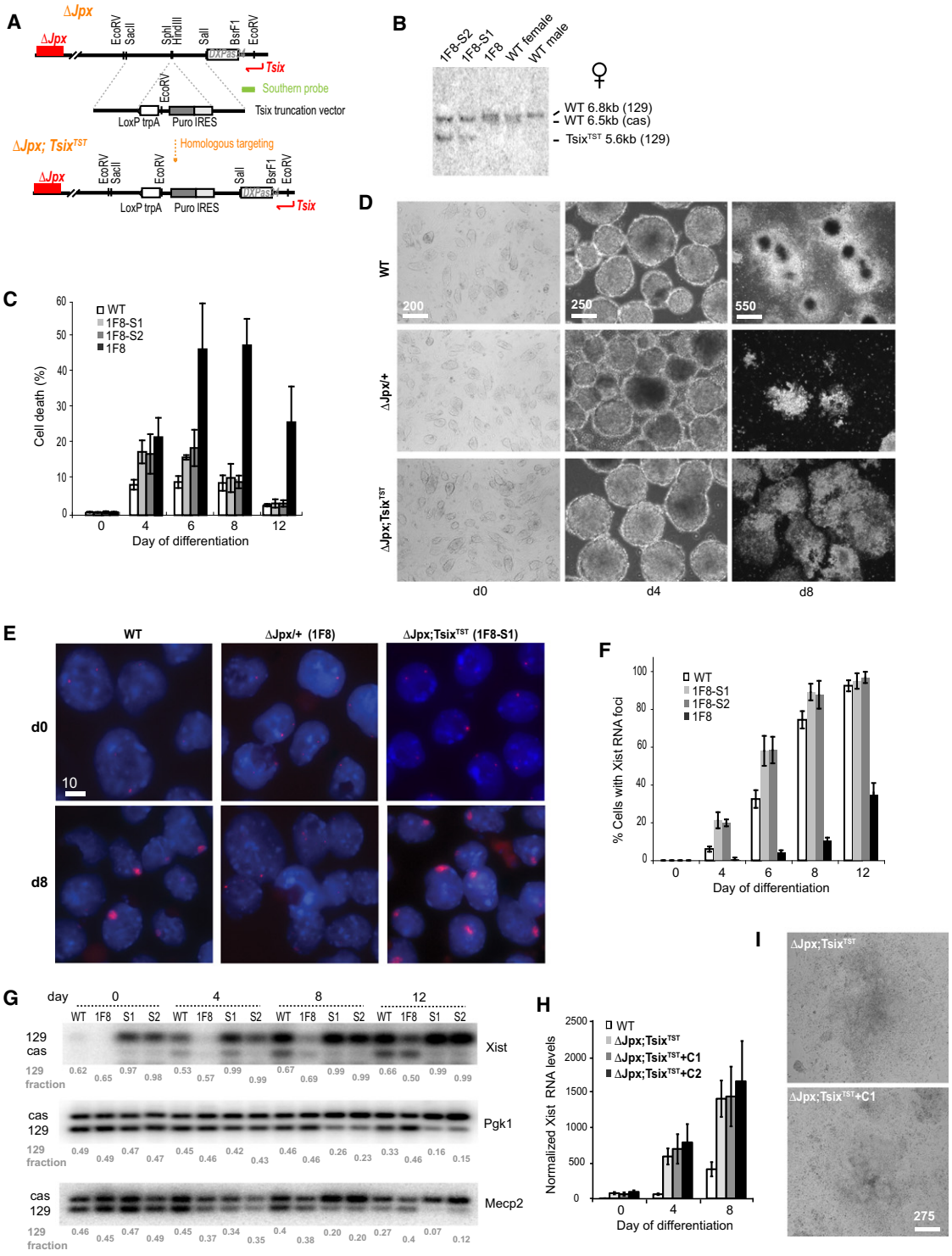

Figure 6. A Tsix RNA Truncation Suppresses *ΔJpx*

(A) Targeting the *Tsix* truncation mutation (*Tsix*^{TST}) (Ogawa et al., 2008) to the *ΔJpx* chromosome in 1F8 female ES cells. *Tsix*^{TST} prematurely terminates Tsix at the targeted triple polyA site (trpA) 1 kb downstream of the major *Tsix* promoter. 1F8-S1 and 1F8-S2 are two independently generated double mutant clones. IRES, internal ribosome entry site. Puro, puromycin selection marker.

(B) Southern analysis using EcoRV digestion to confirm targeting. The X^{129} and X^{cas} alleles have an ~300 bp DXPas34 length polymorphism. The X^{129} allele was targeted in both 1F8-S1 and 1F8-S2.

(C) Cell death analysis shows that *Tsix*^{TST} partially rescues viability of *ΔJpx*/+ ES cells.

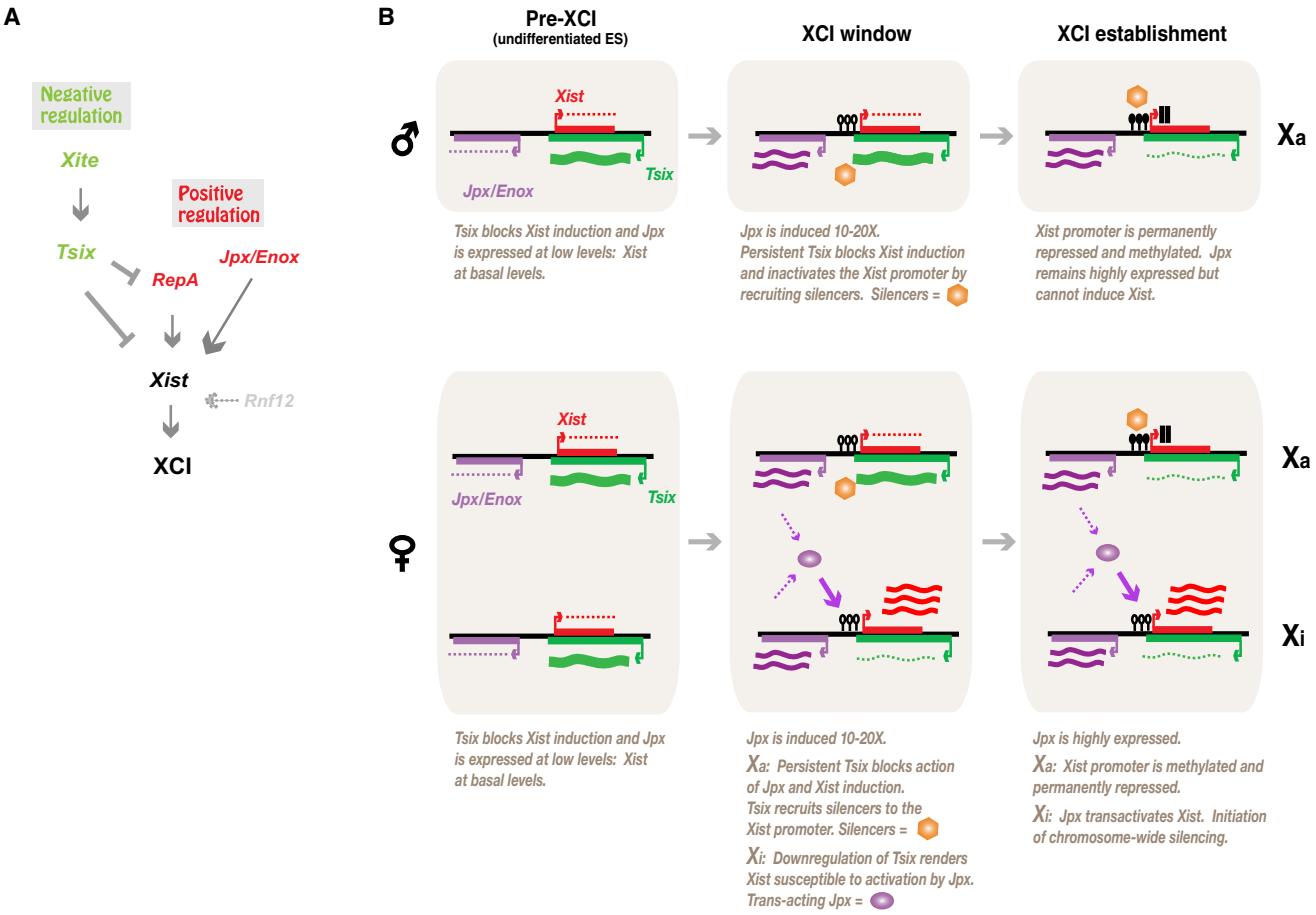

Figure 7. Model and Summary

(A) Proposed epistasis model: *Xist* is under positive-negative regulation by noncoding genes. *Xite* and *Tsix* repress *Xist*, whereas *Jpx* and *RepA* activate *Xist*. Arrows, positive relationship. Blunt arrows, negative relationship. *Rnf12* is a coding gene.

(B) Proposed events in male and female ES cells. *Xist* silencers (orange hexagons) include Dnmt3a and other chromatin modifications. Jpx (purple oval) is depicted as a diffusible *trans*-acting RNA. Open lollipops, unmethylated *Xist* promoter. Filled lollipops, methylated *Xist* promoter.

and JpxUp to generate a 329 bp product, which was digested with NlaIII. End-labeled oligonucleotide, Jpx-P1, GGTGATGTGGGCACTGATCACTCATC, was used as southern probe to recognize both castaneus specific 237 bp and 129 specific 142 bp band. All allelic signals were then quantitated by phosphorimaging.

Luciferase Assay

Promoterless pGL4.19 (Promega) was used to construct luciferase vectors. To generate Jpx-pGL4, a 5.29 kb fragment (nt 92711–98009 of AJ421479), corresponding to the knockout region (promoter, CpG island, and exons 1–2), was cloned into the multiple cloning site. To construct Xist-pGL4, a 4.43 kb fragment (nt 104971–109403 of AJ421479), containing the 500 bp region upstream of *Xist*'s start site and the proximal 4 kb of exon 1, was cloned similarly. Jpx-Xist-pGL4 was constructed by inserting the 5.29 kb Jpx fragment upstream of Xist in Xist-pGL4 vector. Vectors were individually electroporated into female ES cells, and 200–300 stably transfected clones from each vector were pooled and subjected to luciferase assay at different differentiation time points. qRT-PCR for luciferase was performed using primers, Luc-F1, CAGCGCCATTCTACCCACTCG, and Luc-R1, GCTTCTGCCAGCCGAACGC. Beta-actin was amplified as the internal control.

Cell Death Analysis

Cell death assays were performed as described (Stavropoulos et al., 2001). In brief, on d0, both supernatant and attached ES cells were collected and stained with trypan blue dye (Sigma). On other time points, both supernatant and floating embryoid bodies (EBs on d4) or attached EBs (d6 and onward) were collected and stained with trypan blue. The ratios of dead cells (blue) to total cells (i.e., blue dead cells + clear viable cells) were calculated and plotted as a function of time. Each sample was counted in duplicate or triplicate.

(D) Brightfield photographs of wild-type, single, and double mutant female ES cells during differentiation.

(E) RNA FISH indicating that Xist upregulation (large red clouds) is rescued in double mutants.

(F) $Tsix^{TST}$ restores Xist induction in *ΔJpx*/+ cells. Averages ± SD shown for three independent differentiation experiments.

(G) The pattern of allelic skewing is reversed in *ΔJpx;* $Tsix^{TST}$/+ cells.

(H and I) Further depletion of Jpx RNA by shRNA-C knockdown in *ΔJpx;* $Tsix^{TST}$/+ cells did not alter the phenotype of the double mutant, as shown by qRT-PCR of Xist expression (H) and by EB outgrowth to d8 (I). *ΔJpx;* $Tsix^{TST}$/+, 1F8-S2. Two shRNA-C clones derived from 1F8-S2 were examined (C1, C2).

SUPPLEMENTAL INFORMATION

Supplemental Information includes four figures and can be found with this article online at doi:10.1016/j.cell.2010.09.049.

ACKNOWLEDGMENTS

We thank Y. Jeon for providing Xist riboprobes, and A. Chess, D. Lessing, B. Payer, and S. Pinter for critical reading of the manuscript and all members of the laboratory for their helpful input throughout this project. This work was funded by NIH grants K08-HD053824 to D.T., RO1-GM58839 to J.T.L., and a Pathology training grant T32-CA009216. J.T.L. is also an Investigator of the Howard Hughes Medical Institute.

Received: March 19, 2010
Revised: August 6, 2010
Accepted: September 17, 2010
Published: October 28, 2010

REFERENCES

Ahn, J.Y., and Lee, J.T. (2010). Retinoic acid accelerates downregulation of the Xist repressor, Oct4, and increases the likelihood of Xist activation when Tsix is deficient. BMC Dev. Biol. *10*, 90.

Ariel, M., Robinson, E., McCarrey, J.R., and Cedar, H. (1995). Gamete-specific methylation correlates with imprinting of the murine Xist gene. Nat. Genet. *9*, 312–315.

Bacher, C.P., Guggiari, M., Brors, B., Augui, S., Clerc, P., Avner, P., Eils, R., and Heard, E. (2006). Transient colocalization of X-inactivation centres accompanies the initiation of X inactivation. Nat. Cell Biol. *8*, 293–299.

Brockdorff, N., Ashworth, A., Kay, G.F., McCabe, V.M., Norris, D.P., Cooper, P.J., Swift, S., and Rastan, S. (1992). The product of the mouse Xist gene is a 15 kb inactive X-specific transcript containing no conserved ORF and located in the nucleus. Cell *71*, 515–526.

Brown, C.J., Lafreniere, R.G., Powers, V.E., Sebastio, G., Ballabio, A., Pettigrew, A.L., Ledbetter, D.H., Levy, E., Craig, I.W., and Willard, H.F. (1991). Localization of the X inactivation centre on the human X chromosome in Xq13. Nature *349*, 82–84.

Brown, C.J., Hendrich, B.D., Rupert, J.L., Lafreniere, R.G., Xing, Y., Lawrence, J., and Willard, H.F. (1992). The human XIST gene: analysis of a 17 kb inactive X-specific RNA that contains conserved repeats and is highly localized within the nucleus. Cell *71*, 527–542.

Cattanach, B.M., and Isaacson, J.H. (1967). Controlling elements in the mouse X chromosome. Genetics *57*, 331–346.

Chow, J.C., Hall, L.L., Clemson, C.M., Lawrence, J.B., and Brown, C.J. (2003). Characterization of expression at the human XIST locus in somatic, embryonal carcinoma, and transgenic cell lines. Genomics *82*, 309–322.

Chureau, C., Prissette, M., Bourdet, A., Barbe, V., Cattolico, L., Jones, L., Eggen, A., Avner, P., and Duret, L. (2002). Comparative sequence analysis of the X-inactivation center region in mouse, human, and bovine. Genome Res. *12*, 894–908.

Clemson, C.M., Hall, L.L., Byron, M., McNeil, J., and Lawrence, J.B. (2006). The X chromosome is organized into a gene-rich outer rim and an internal core containing silenced nongenic sequences. Proc. Natl. Acad. Sci. USA *103*, 7688–7693.

Davidow, L.S., Breen, M., Duke, S.E., Samollow, P.B., McCarrey, J.R., and Lee, J.T. (2007). The search for a marsupial XIC reveals a break with vertebrate synteny. Chromosome Res. *15*, 137–146.

Donohoe, M.E., Silva, S.S., Pinter, S.F., Xu, N., and Lee, J.T. (2009). The pluripotency factor Oct4 interacts with Ctcf and also controls X-chromosome pairing and counting. Nature *460*, 128–132.

Duret, L., Chureau, C., Samain, S., Weissenbach, J., and Avner, P. (2006). The Xist RNA gene evolved in eutherians by pseudogenization of a protein-coding gene. Science *312*, 1653–1655.

Hoki, Y., Kimura, N., Kanbayashi, M., Amakawa, Y., Ohhata, T., Sasaki, H., and Sado, T. (2009). A proximal conserved repeat in the Xist gene is essential as a genomic element for X-inactivation in mouse. Development *136*, 139–146.

Hore, T.A., Koina, E., Wakefield, M.J., and Marshall Graves, J.A. (2007). The region homologous to the X-chromosome inactivation centre has been disrupted in marsupial and monotreme mammals. Chromosome Res. *15*, 147–161.

Huynh, K.D., and Lee, J.T. (2003). Inheritance of a pre-inactivated paternal X chromosome in early mouse embryos. Nature *426*, 857–862.

Johnston, C.M., Newall, A.E., Brockdorff, N., and Nesterova, T.B. (2002). Enox, a novel gene that maps 10 kb upstream of Xist and partially escapes X inactivation. Genomics *80*, 236–244.

Jonkers, I., Barakat, T.S., Achame, E.M., Monkhorst, K., Kenter, A., Rentmeester, E., Grosveld, F., Grootegoed, J.A., and Gribnau, J. (2009). RNF12 is an X-encoded dose-dependent activator of X chromosome inactivation. Cell *139*, 999–1011.

Koerner, M.V., Pauler, F.M., Huang, R., and Barlow, D.P. (2009). The function of non-coding RNAs in genomic imprinting. Development *136*, 1771–1783.

Lee, J.T. (2000). Disruption of imprinted X inactivation by parent-of-origin effects at Tsix. Cell *103*, 17–27.

Lee, J.T. (2005). Regulation of X-chromosome counting by Tsix and Xite sequences. Science *309*, 768–771.

Lee, J.T. (2009). Lessons from X-chromosome inactivation: long ncRNA as guides and tethers to the epigenome. Genes Dev. *23*, 1831–1842.

Lee, J.T., and Lu, N. (1999). Targeted mutagenesis of Tsix leads to nonrandom X inactivation. Cell *99*, 47–57.

Lee, J.T., Davidow, L.S., and Warshawsky, D. (1999a). Tsix, a gene antisense to Xist at the X-inactivation centre. Nat. Genet. *21*, 400–404.

Lee, J.T., Lu, N., and Han, Y. (1999b). Genetic analysis of the mouse X inactivation center defines an 80-kb multifunction domain. Proc. Natl. Acad. Sci. USA *96*, 3836–3841.

Lucchesi, J.C., Kelly, W.G., and Panning, B. (2005). Chromatin remodeling in dosage compensation. Annu. Rev. Genet. *39*, 615–651.

Luikenhuis, S., Wutz, A., and Jaenisch, R. (2001). Antisense transcription through the Xist locus mediates Tsix function in embryonic stem cells. Mol. Cell. Biol. *21*, 8512–8520.

Lyon, M.F. (1961). Gene action in the X-chromosome of the mouse (Mus musculus L.). Nature *190*, 372–373.

Marahrens, Y., Panning, B., Dausman, J., Strauss, W., and Jaenisch, R. (1997). Xist-deficient mice are defective in dosage compensation but not spermatogenesis. Genes Dev. *11*, 156–166.

Mercer, T.R., Dinger, M.E., and Mattick, J.S. (2009). Long non-coding RNAs: insights into functions. Nat. Rev. Genet. *10*, 155–159.

Monk, M., and Harper, M.I. (1979). Sequential X chromosome inactivation coupled with cellular differentiation in early mouse embryos. Nature *281*, 311–313.

Monkhorst, K., Jonkers, I., Rentmeester, E., Grosveld, F., and Gribnau, J. (2008). X inactivation counting and choice is a stochastic process: evidence for involvement of an x-linked activator. Cell *132*, 410–421.

Morey, C., Navarro, P., Debrand, E., Avner, P., Rougeulle, C., and Clerc, P. (2004). The region 3′ to Xist mediates X chromosome counting and H3 Lys-4 dimethylation within the Xist gene. EMBO J. *23*, 594–604.

Namekawa, S.H., Payer, B., Huynh, K.D., Jaenisch, R., and Lee, J.T. (2010). Two-step imprinted X inactivation: repeat versus genic silencing in the mouse. Mol. Cell. Biol. *30*, 3187–3205.

Navarro, P., Pichard, S., Ciaudo, C., Avner, P., and Rougeulle, C. (2005). Tsix transcription across the Xist gene alters chromatin conformation without affecting Xist transcription: implications for X-chromosome inactivation. Genes Dev. *19*, 1474–1484.

Navarro, P., Chambers, I., Karwacki-Neisius, V., Chureau, C., Morey, C., Rougeulle, C., and Avner, P. (2008). Molecular coupling of Xist regulation and pluripotency. Science *321*, 1693–1695.

Nicodemi, M., and Prisco, A. (2007). Symmetry-breaking model for X-chromosome inactivation. Phys. Rev. Lett. *98*, 108104.

Norris, D.P., Patel, D., Kay, G.F., Penny, G.D., Brockdorff, N., Sheardown, S.A., and Rastan, S. (1994). Evidence that random and imprinted Xist expression is controlled by preemptive methylation. Cell *77*, 41–51.

Ogawa, Y., and Lee, J.T. (2003). Xite, X-inactivation intergenic transcription elements that regulate the probability of choice. Mol. Cell *11*, 731–743.

Ogawa, Y., Sun, B.K., and Lee, J.T. (2008). Intersection of the RNA Interference and X-Inactivation Pathways. Science *320*, 1336–1341.

Ohhata, T., Hoki, Y., Sasaki, H., and Sado, T. (2006). Tsix-deficient X chromosome does not undergo inactivation in the embryonic lineage in males: implications for Tsix-independent silencing of Xist. Cytogenet. Genome Res. *113*, 345–349.

Ohhata, T., Hoki, Y., Sasaki, H., and Sado, T. (2008). Crucial role of antisense transcription across the Xist promoter in Tsix-mediated Xist chromatin modification. Development *135*, 227–235.

Payer, B., and Lee, J.T. (2008). X Chromosome Dosage Compensation: How Mammals Keep the Balance. Annu. Rev. Genet. *42*, 733–772.

Penny, G.D., Kay, G.F., Sheardown, S.A., Rastan, S., and Brockdorff, N. (1996). Requirement for Xist in X chromosome inactivation. Nature *379*, 131–137.

Plath, K., Fang, J., Mlynarczyk-Evans, S.K., Cao, R., Worringer, K.A., Wang, H., de la Cruz, C.C., Otte, A.P., Panning, B., and Zhang, Y. (2003). Role of histone H3 lysine 27 methylation in X inactivation. Science *300*, 131–135.

Sado, T., Wang, Z., Sasaki, H., and Li, E. (2001). Regulation of imprinted X-chromosome inactivation in mice by Tsix. Development *128*, 1275–1286.

Sado, T., Hoki, Y., and Sasaki, H. (2005). Tsix silences Xist through modification of chromatin structure. Dev. Cell *9*, 159–165.

Schoeftner, S., Sengupta, A.K., Kubicek, S., Mechtler, K., Spahn, L., Koseki, H., Jenuwein, T., and Wutz, A. (2006). Recruitment of PRC1 function at the initiation of X inactivation independent of PRC2 and silencing. EMBO J. *25*, 3110–3122.

Shevchenko, A.I., Zakharova, I.S., Elisaphenko, E.A., Kolesnikov, N.N., Whitehead, S., Bird, C., Ross, M., Weidman, J.R., Jirtle, R.L., Karamysheva, T.V., et al. (2007). Genes flanking Xist in mouse and human are separated on the X chromosome in American marsupials. Chromosome Res. *15*, 127–136.

Silva, J., Mak, W., Zvetkova, I., Appanah, R., Nesterova, T.B., Webster, Z., Peters, A.H., Jenuwein, T., Otte, A.P., and Brockdorff, N. (2003). Establishment of histone h3 methylation on the inactive X chromosome requires transient recruitment of Eed-Enx1 polycomb group complexes. Dev. Cell *4*, 481–495.

Simmler, M.C., Cunningham, D.B., Clerc, P., Vermat, T., Caudron, B., Cruaud, C., Pawlak, A., Szpirer, C., Weissenbach, J., Claverie, J.M., et al. (1996). A 94 kb genomic sequence 3′ to the murine Xist gene reveals an AT rich region containing a new testis specific gene Tsx. Hum. Mol. Genet. *5*, 1713–1726.

Starmer, J., and Magnuson, T. (2009). A new model for random X chromosome inactivation. Development *136*, 1–10.

Stavropoulos, N., Lu, N., and Lee, J.T. (2001). A functional role for Tsix transcription in blocking Xist RNA accumulation but not in X-chromosome choice. Proc. Natl. Acad. Sci. USA *98*, 10232–10237.

Sun, B.K., Deaton, A.M., and Lee, J.T. (2006). A transient heterochromatic state in Xist preempts X inactivation choice without RNA stabilization. Mol. Cell *21*, 617–628.

Tsai, C.L., Rowntree, R.K., Cohen, D.E., and Lee, J.T. (2008). Higher order chromatin structure at the X-inactivation center via looping DNA. Dev. Biol. *319*, 416–425.

Vigneau, S., Augui, S., Navarro, P., Avner, P., and Clerc, P. (2006). An essential role for the DXPas34 tandem repeat and Tsix transcription in the counting process of X chromosome inactivation. Proc. Natl. Acad. Sci. USA *103*, 7390–7395.

Wan, L.B., and Bartolomei, M.S. (2008). Regulation of imprinting in clusters: noncoding RNAs versus insulators. Adv. Genet. *61*, 207–223.

Wutz, A., and Gribnau, J. (2007). X inactivation Xplained. Curr. Opin. Genet. Dev. *17*, 387–393.

Wutz, A., Rasmussen, T.P., and Jaenisch, R. (2002). Chromosomal silencing and localization are mediated by different domains of Xist RNA. Nat. Genet. *30*, 167–174.

Xu, N., Tsai, C.L., and Lee, J.T. (2006). Transient homologous chromosome pairing marks the onset of X inactivation. Science *311*, 1149–1152.

Yang, Y., and Seed, B. (2003). Site-specific gene targeting in mouse embryonic stem cells with intact bacterial artificial chromosomes. Nat. Biotechnol. *21*, 447–451.

Zhao, J., Sun, B.K., Erwin, J.A., Song, J.J., and Lee, J.T. (2008). Polycomb proteins targeted by a short repeat RNA to the mouse X chromosome. Science *322*, 750–756.

Zuccotti, M., and Monk, M. (1995). Methylation of the mouse Xist gene in sperm and eggs correlates with imprinted Xist expression and paternal X-inactivation. Nat. Genet. *9*, 316–320.

Supplemental Information

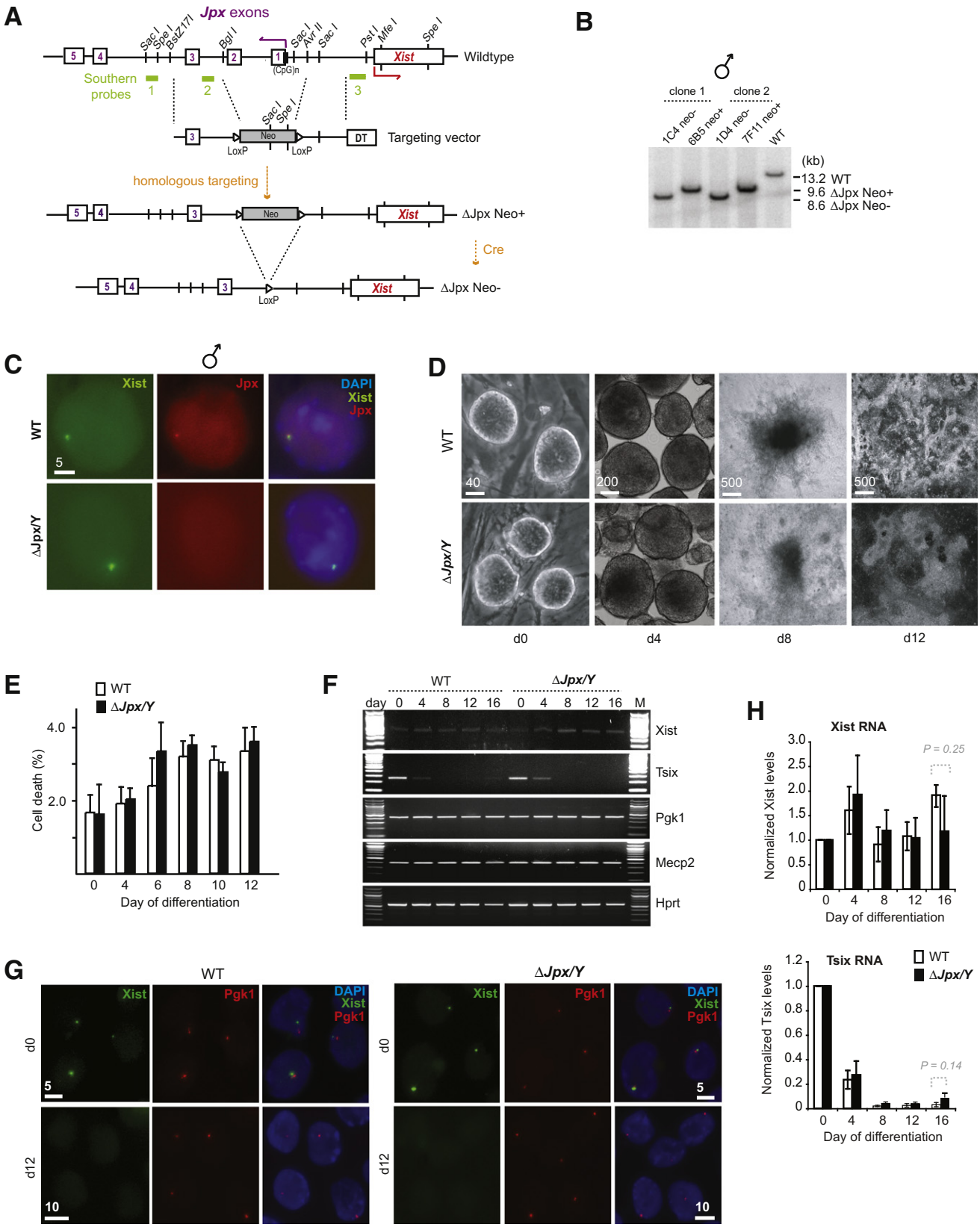

Figure S1. *ΔJpx* Has No Effects in Male Cells

(A) The *Jpx* gene, targeting vector, and products of homologous targeting before and after Cre-mediated excision of the *Neo* positive-selection marker. DT, diphtheria toxin for negative selection. (CpG)n, CpG island. The numbered boxes represent five *Jpx* exons.

(B) Southern analysis of SacI-digested genomic DNA from *Jpx* knockout male ES clones using probe 1. Wildtype (WT), two Neo+ mutants, and the derivative Neo− clones for the *Jpx* knockout are shown. The Neo− male clones, 1C4 and 1D4, were derived from the Neo+ 6B5 and 7F11 clones, respectively, by Cre-mediated excision.

(C) DNA FISH of wildtype and Δ*Jpx*/Y cells. *Xist* probe (pSx9), FITC-labeled (green). The *Jpx* probe (Cy3-labelled, red) is located in the region of deletion.

(D) Brightfield photographs of undifferentiated (d0) and differentiated (d4-d12) *ΔJpx*/Y and WT ES cells. ES cells were differentiated by EB suspension culture for 4 days and plated on gelatin-coated petridishes after d4.

(E) Cell death plots of WT and *ΔJpx*/+ ES cells, with averages and standard errors (SE) from three independent differentiation experiments. Trypan-blue exclusion method is based on the fact that dead cells take up the dye, whereas viable cells exclude it. % cell death = ([blue cells] / [blue cells + clear cells]) × 100. Sample size (n) = 150–200 for d0 timepoints, 500–2000 cells for all other timepoints.

(F) RT-PCR analysis of indicated transcripts from d0-d16. EtBr-stained gels are shown. M, 100 bp markers.

(G) Two-color RNA FISH for Xist and Pgk1 expression. Xist probe, FITC-labeled pSx9. Pgk1 probe, Cy3-labeled pCAB17.

(H) Real-time qRT-PCR of Xist and Tsix RNA in WT and mutant male cells. RNA levels were normalized to that of β-actin. Averages and SE for six independent differentiation experiments are shown for each RNA. *P*, calculated by pairwise comparison using the Student's *t* test. Differences were insignificant for all days, shown only for d16.

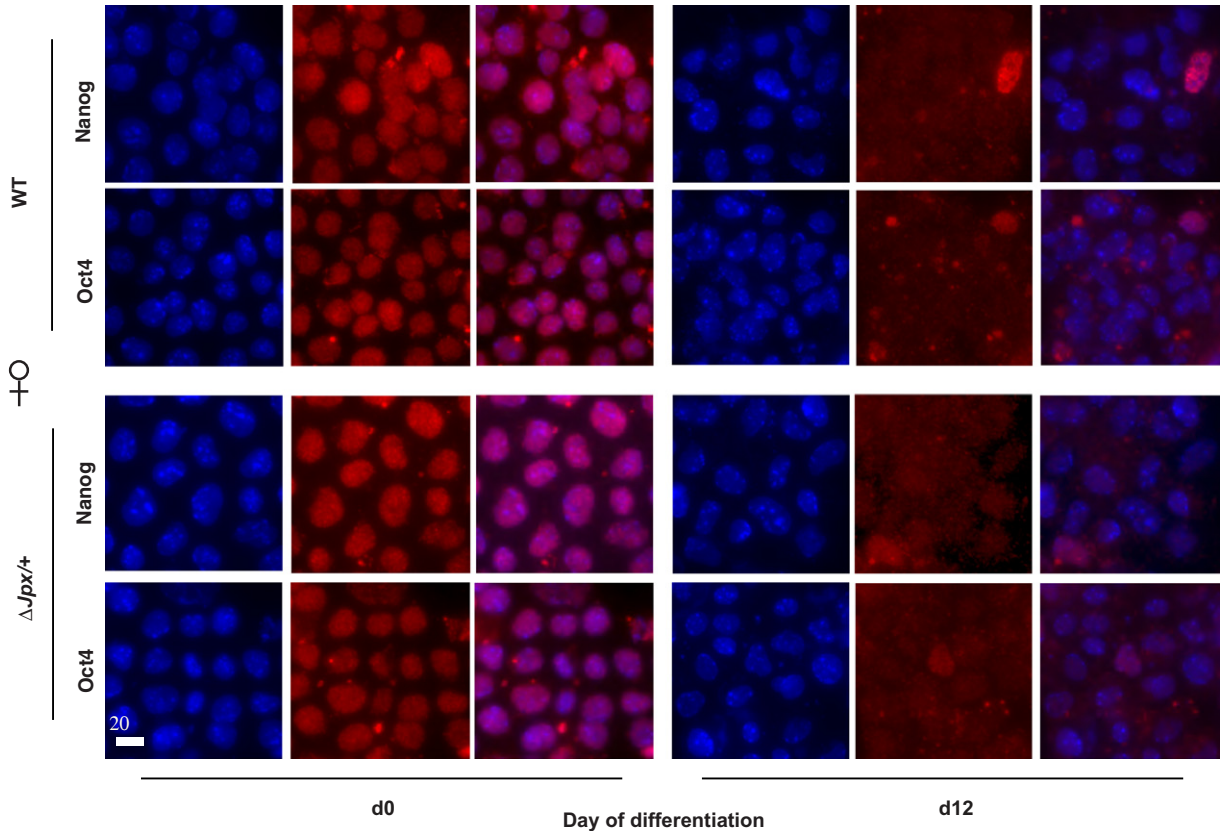

Figure S2. Immunostaining for Oct4 and Nanog Demonstrate Appropriate Downregulation of Stem Cell Markers during Differentiation of *ΔJpx/+* Cells

WT and *ΔJpx/+* female ES cells were immunostained for Oct4 and Nanog on d0 and d12 of differentiation. In each case, ES colonies appropriately expressed Oct4 and Nanog in the undifferentiated and the EB derivatives appropriately lost the pluripotency markers by d12 of differentiation.

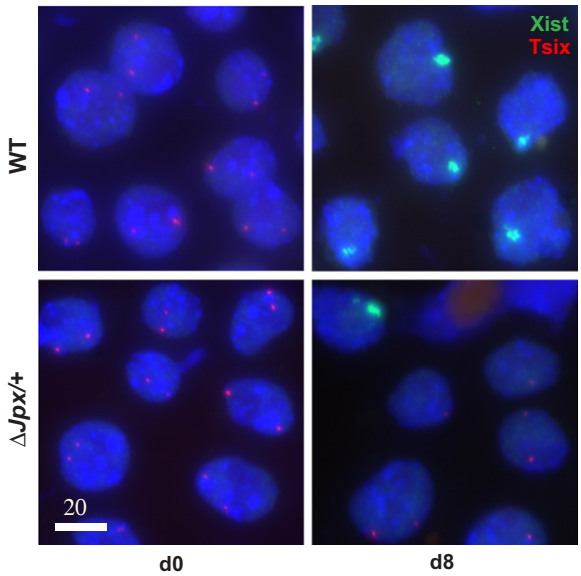

Figure S3. Strand-Specific RNA FISH Analysis of Xist and Tsix RNA

Wild-type and mutant female ES cells were subjected to two-color strand-specific RNA FISH analysis to confirm Xist and Tsix origins of large RNA clouds and pinpoint signals, respectively. Xist probe (green), riboprobe cocktail. Tsix probe (red), pCC3.

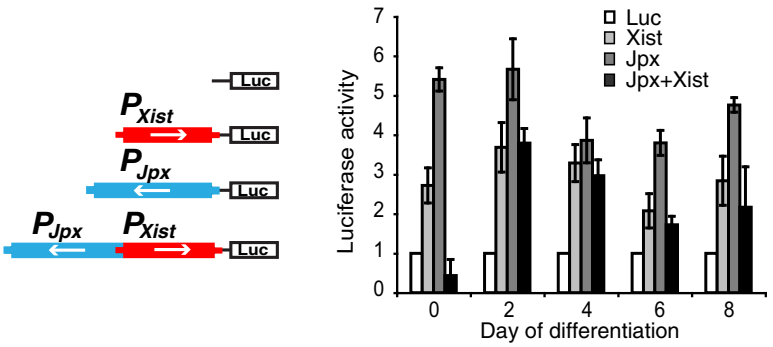

Figure S4. *Jpx* Does Not Obviously Act as an Enhancer for *Xist*

Luciferase (Luc) assay to test the ability of *Jpx* to enhance expression from the *Xist* promoter.